Journal of Applied Electrochemistry **31**: 25–34, 2001.

A study of hardness and grain size in pulse current electroforming of nickel using different shaped waveforms

K.P. WONG, K.C. CHAN* and T.M. YUE
Department of Manufacturing Engineering, The Hong Kong Polytechnic University, Hung Hom, Kowloon, Hong Kong
*(*author for correspondence, fax: (852) 23625267, e-mail: mfkcchan@polyu.edu.hk)*

Received 12 May 1999; accepted in revised form 23 May 2000

Key words: grain size, hardness, pulse current electroforming, shaped waveform

Abstract

This paper describes an experimental and theoretical study of the effects of different types of waveform on the grain size and the hardness of nickel electroforms in pulse current electroforming. The highest hardness value and the finest grain size were obtained using a ramp-down waveform with relaxation time. The experimental results show that compared with the conventional rectangular waveform and with relaxation time, the hardness value can be improved by about 28% when a ramp-down waveform, also with relaxation time, is used. These results are supported by theoretical predictions and the study of the surface morphology of the electroforms by scanning electron microscopy.

List of symbols

b	shape factor relating to the surface area (i.e., $b = P^2/4S$; e.g., $b = \pi$ for a circular nucleus)
c	concentration
c_e	interfacial concentration
c_0	bulk concentration
d	grain size
D	diffusion coefficient
e	charge of an electron
F	faradaic constant
G	grain size
H	hardness value
H_0	a value determined by dislocation blocking
i	current density
i_0	exchange current
i_a	anodic peak current density
i_c	cathodic peak current density
i_{av}	average current density
i_L	limiting current density
k	Boltzmann's constant
k_1	a proportionality constant
k_2	related to the amount of energy needed for the two-dimensional nucleation
K_H	penetrability of the moving dislocation boundary
m	number of cycles
N	number of ions contained in a cluster
N_c	size of the critical nucleus
P	perimeter
r	t_a/t_c
R	gas constant
s	area occupied by one atom on the surface on the nucleus
S	surface area
t	time
t_a	pause time
t_c	cathodic time of mandrel
T	temperature
J	nucleation rate
W	waveform
x	coordinate in the horizontal direction
z	number of electrons

Greek symbols

θ	period of one cycle
δ	total thickness of diffusion layer
α	transfer coefficient
ε	specific edge energy
η	total overpotential
η_0	ohmic overpotential
η_s	surface overpotential
η_c	concentration overpotential
ΔG	free energy of formation of a cluster
$\Phi(N)$	increase of the surface energy due to creation of the surface of a cluster

Suffixes

rec	due to applying rectangular waveform with relaxation time
rup	due to applying ramp-up waveform with relaxation time

rdn due to applying ramp-down waveform with relaxation time
tri due to applying triangular waveform with relaxation time

1. Introduction

The main practical advantage of pulse-current electroforming is its potential to improve the properties of electroforms. Encouraging results have been reported [1–5]. Despic [6] and Romanov [7] have shown that the formation of zinc dendrites in sulfate baths is greatly reduced by pulse current electroforming, with smoother and denser electroforms obtained. Avila and Brown [8] have reported that pulse current electroforming allows a reduction by half in the amount of gold needed for the coatings of integrated circuits, without impairing the conductivity. Moreover, the considerable quantities of additives used in electroforming baths can be reduced by pulse current electroforming [5, 8, 9].

Although it has been demonstrated that the quality of electroforms can be improved by using pulse current with rectangular waveform [4, 9–11], there has been no reported work on the use of different shaped waveforms. Since nickel coatings enhance the value and usefulness of industrial equipment and components, investigations on improving the properties of nickel electroforms are therefore of high significance [5, 12, 13].

Recently, much attention has been paid to hardness and grain size investigations [14, 15]. The value of hardness is a commonly used quantity which can give a general indication of the strength of the material as well as its resistance to wear and scratching [16–21]. A fine-grained material is harder and stronger than a coarse-grained material, since the former has a greater total grain boundary area to impede dislocation motion. It has also been found that for some metals, the value of hardness is proportional to the reciprocal square root of the average grain diameter [17, 22]. Since the effect of using different types of shaped pulse current on the hardness and the grain size of electroforms has not yet been fully explored, it is worth paying attention to this area.

In this work, the relationship between the grain size and the hardness of nickel electroforms produced by utilizing different types of waveform was studied. The different types of shaped waveform used were (a) a rectangular waveform with relaxation time, (b) a ramp-up waveform with relaxation time, (c) a ramp-down waveform with relaxation time and (d) a triangular waveform with relaxation time.

2. Theoretical consideration

2.1. *Hardness and grain size*

In an attempt to quantitatively relate the grain size in a metal to its mechanical properties, Petch and Hall proposed [23, 24] an expression relating grain size, d, with hardness, H, in a metal. Hardness is defined in this case as the yield stress (i.e., the level of stress at which the material experiences the onset of permanent deformation). Thus

$$H = H_0 + K_{\mathrm{H}} \frac{1}{\sqrt{d}} \tag{1}$$

where H_0 and K_{H} are determined experimentally for a given specific metal and where their physical meanings are as follows: H_0 is the value determined by dislocation blocking, which is, in turn, dependent on the friction stress; and K_{H} represents the penetrability of the moving dislocation boundary. This is related to the available slip systems.

This useful empirical expression is applicable to many electrodeposited materials [24, 25]. The expression has been able, for instance, to provide an explanation for the phenomenon of brittle cracking in chromium electrodeposits. It has been useful in understanding of the functional connection between hardness and grain size values in many electrodeposits.

2.2. *Instantaneous concentration profile of electroactive ions in the diffusion layer*

Viswanathan et al. [26] have shown that the simplified diffusion model used by Cheh [27] can adequately predict the concentration of the reacting species at the electrode surface once the flux of the reacting species is specified. The simplified diffusion model neglects the convection term in the differential equation, but replaces the boundary condition at infinity by an approximate condition at the outer edge of the Nernst diffusion layer. Consequently, the concentration of the reacting species is described by the following diffusion equation:

$$\frac{\partial c}{\partial t} = D \frac{\partial^2 c}{\partial x^2} \tag{2}$$

with the initial and boundary conditions:

$$c(0, x) = c_0 \tag{3}$$

$$c(t, \delta) = c_0 \tag{4}$$

$$\left.\frac{\partial c}{\partial x}\right|_{x=0} = \frac{i(t)}{zFD} \tag{5}$$

For a special case in which the applied current is constant, Equation 2 (subject to the initial and boundary conditions of Equations 3–5) can be solved by the Fourier series method [28]:

$$c_{\mathrm{e}} - c_0 = \frac{ix}{zFD} + \frac{8i\delta}{zFD\pi^2} \sum_{n=1}^{\infty} \frac{(-1)^n}{(2n-1)^2}$$

$$\times \exp\left(-\frac{(2n-1)^2\pi^2 Dt}{4\delta^2}\right)\sin\left(\frac{(2n-1)\pi}{2\delta}\right) \tag{6}$$

For the sake of brevity, Equation 6 may be written as

$$c_e - c_0 = Cx + \frac{8C\delta}{\pi^2}\sum_{n=1}^{\infty}\frac{(-1)^n}{p^2}\exp(-p^2 at)\sin(pgx) \tag{7}$$

where $n = 1, 2, 3, 4, 5, 6, 7, 8\ldots$

$$p = 2n - 1 \tag{8}$$

$$g = \frac{\pi}{2\delta} \tag{9}$$

$$a = \frac{\pi^2 D}{4\delta^2} \tag{10}$$

$$C = \frac{i}{zFD} \tag{11}$$

because $(-1)^n \sin(pgx) = -\cos[pg(\delta - x)]$

So,

$$c_e - c_0 = Cx - \frac{8C\delta}{\pi^2}\sum_{n=1}^{\infty}\frac{1}{p^2}\exp(-p^2 at)\cos(pg\xi) \tag{12}$$

where

$$\xi = \delta - x \tag{13}$$

Equation 12 is applicable only when the current remains constant during electrolysis. It is now proposed to deal with the more general case where the currents i_1, i_2, i_3, corresponding to C_1, C_2, C_3, etc., act successively. C_1 is obtained from $t = 0$ to $t = t_1$, C_2 is obtained from t_1 to t_2, and C_3 is obtained from t_2 to t_3, etc.

At $t = 0$, $c = c_0$ for all values of x. Up to the moment t_1, the value of $(c_e - c_0)$ is given by Equation 12. In particular,

for $t = t_1$,

$$\begin{aligned} c_e - c_0 &= C_1 x - \frac{8C_1\delta}{\pi^2}\sum_{n=1}^{\infty}\frac{1}{p^2}\exp(-p^2 at_1)\cos(pg\xi) \\ &= C_2 x + (C_1 - C_2)x - \frac{8C_1\delta}{\pi^2} \\ &\quad \times \sum_{n=1}^{\infty}\frac{1}{p^2}\exp(-p^2 at_1)\cos(pg\xi) \\ &= C_2 x - \frac{8\delta}{\pi^2}\sum_{n=1}^{\infty}\frac{1}{p^2}[C_1\exp(-p^2 at_1) \\ &\quad + (C_2 - C_1)]\cos(pg\xi) \end{aligned} \tag{14}$$

for $t_1 < t < t_2$,

$$\begin{aligned} c_e - c_0 &= C_2 x - \frac{8\delta}{\pi^2}\sum_{n=1}^{\infty}\frac{1}{p^2}[C_1\exp(-p^2 at_1) \\ &\quad + (C_2 - C_1)]\exp[-p^2 a(t - t_1)]\cos(pg\xi) \end{aligned} \tag{15}$$

Generally, for $t_{r-1} < t < t_r$, the Equation 7 can be written as

$$\begin{aligned} c_e - c_0 = C_r x - \frac{8\delta}{\pi^2}\{&C_1\exp(-p^2 at) + (C_2 - C_1) \\ &\times \exp[-p^2 a(t - t_1)] + \cdots + (C_k - C_{k-1}) \\ &\times \exp[-p^2 a(t - t_{k-1})] + \cdots + (C_r - C_{r-1}) \\ &\times \exp[-p^2 a(t - t_{r-1})]\}\cos(pg\xi) \end{aligned}$$

So,

$$\begin{aligned} c_e - c_0 = C_r x - \frac{8\delta}{\pi^2}\sum_{n=1}^{\infty}\frac{1}{p^2}&\left\{C_1\exp(-p^2 at)\right. \\ &\left. + \sum_{k=1}^{r}(C_k - C_{k-1})\exp[-p^2 a(t - t_{k-1})]\right\} \\ &\times \cos(pg\xi) \end{aligned} \tag{16}$$

Alternatively, the braced expression { } can be rearranged, and so,

$$\begin{aligned} c_e - c_0 = C_r x - \frac{8\delta}{\pi^2}\sum_{n=1}^{\infty}\frac{1}{p^2}&\left\{(C_r x)\exp[-p^2 a(t - t_{r-1})]\right. \\ &+ \sum_{k=1}^{r-1}[(C_k x)\exp[-p^2 a(t - t_{k-1})] \\ &\left. - \exp[-p^2 a(t - t_k)]]\right\}\cos(pg\xi) \end{aligned} \tag{17}$$

If the difference between any two successive constant currents is infinitely small, and the number of currents is infinite, the difference $(C_k - C_{k-1})$ in Equation 16 becomes a differential, and the summation with respect to k becomes an integration. When u is written in place of t_k, and if the applied current varies with time (i.e., $C = i(t)/zFD$), then Equation 16 becomes:

$$\begin{aligned} c_e - c_0 &= \frac{i(t)x}{zFD} - \frac{2D}{\delta}\sum_{n=1}^{\infty}\left\{\frac{i(t)}{ap^2 zFD} - \exp(-p^2 at)\right. \\ &\quad \left.\times \int_0^t \exp(p^2 au)i(u)\mathrm{d}u\right\}\cos(pg\xi) \\ &= \frac{2D}{\delta}\sum_{n=1}^{\infty}\left[\exp(-p^2 at)\int_0^t \exp(p^2 au)i(u)\mathrm{d}u\right] \\ &\quad \times \cos(pg\xi) \end{aligned} \tag{18}$$

Equation 18 represents the change in concentration profile of electroactive ions within the diffusion layer at any time, or the change in the concentration at any position inside the diffusion layer.

By letting $x = \delta$ in Equation 18, the change in concentration of electroactive ions is obtained:

$$c_e - c_0 = \frac{2D}{\delta}\sum_{n=1}^{\infty}\left[\exp(-p^2at)\int_0^t \exp(p^2au)i(u)\mathrm{d}u\right] \tag{19}$$

The Equation 19 can be rewritten as

$$\frac{c_e}{c_0} = 1 + \frac{2D}{\delta c_0}\sum_{n=1}^{\infty}\left[\exp(-p^2at)\int_0^t \exp(p^2au)i(u)\mathrm{d}u\right] \tag{20}$$

The relationship between current density and the shaped waveform can be described by the following equations:

(a) *For a rectangular waveform with relaxation time*, W_{rec}

$$i(t) = \begin{cases} i_c & \text{for } m\theta < t \leqslant \left(m + \frac{1}{r+1}\right)\theta \\ 0 & \text{for } \left(m + \frac{1}{r+1}\right)\theta < t \leqslant (m+1)\theta \end{cases} \tag{21}$$

$$i_{av} = \frac{i_c \times t_c}{t_c + t_a} = \frac{i_c}{r+1} \tag{22}$$

So,

$$i_c = 2i_{av} \quad \text{if } t_a = t_c \tag{23}$$

During the cathodic time of mandrel, $0 < t \leqslant t_c$,

$$i(u) = \frac{i_c}{zFD} \tag{24}$$

By substituting Equation 24 into Equation 20, the change in concentration is

$$\frac{c_e}{c_0} = 1 + \frac{8}{\pi^2}\frac{i_c\delta}{zFc_0D}\sum_{n=1}^{\infty}\frac{1-\exp(-p^2at)}{p^2} \tag{25}$$

During the pause time, $t_c < t \leqslant t_a$,

$$i(u) = 1 \tag{26}$$

Due to sufficiently high frequencies (i.e., sufficiently small period of pulsation) the surface concentration of depositing ions does not vary with time [29, 30]. The surface concentration at the end of the cathodic pulse is the same as that at the end of the anodic pulse, that is, the change of concentration is found at $t = t_c$:

$$\frac{c_e}{c_0} = 1 + \frac{2i_c}{zFc_0\delta}\sum_{n=1}^{\infty}\frac{\exp[-p^2a(t-t_c)] - \exp(-p^2at)}{p^2a} \tag{27}$$

(b) *For a ramp-up waveform with relaxation time*, W_{rup}

$$i(t) = \begin{cases} \frac{2i_ct}{\theta} - 2mi_c & \text{for } m\theta < t \leqslant \left(m + \frac{1}{r+1}\right)\theta \\ 0 & \text{for } \left(m + \frac{1}{r+1}\right)\theta < t \leqslant (m+1)\theta \end{cases} \tag{28}$$

$$i_{av} = \frac{1}{2} \times \frac{i_c \times t_c}{t_c + t_a} = \frac{1}{2} \times \frac{i_c}{r+1} \tag{29}$$

So,

$$i_c = 4i_{av} \quad \text{if} \quad t_a = t_c \tag{30}$$

During the cathodic time of mandrel, $0 < t \leqslant t_c$,

$$i(u) = \frac{i_c}{zFD} \times \frac{2u}{\theta} \tag{31}$$

By substituting Equation 31 into Equation 20, the change in concentration is

$$\frac{c_e}{c_0} = 1 + \frac{4i_c}{zFc_0\delta}\sum_{n=1}^{\infty}\frac{1}{p^4a^2\theta}[p^2at - 1 + \exp(-p^2at)] \tag{32}$$

During the pause time, $t_c < t \leqslant t_a$, the change in concentration is found to be the same as in Equation 27.

(c) *For a ramp-down waveform with relaxation time*, W_{rdn}

$$i(t) = \begin{cases} \frac{-2i_ct}{\theta} + i_c + 2mi_c \\ \quad \text{for } m\theta < t \leqslant \left(m + \frac{1}{r+1}\right)\theta \\ 0 \quad \text{for } \left(m + \frac{1}{r+1}\right)\theta < t \leqslant (m+1)\theta \end{cases} \tag{33}$$

$$i_{av} = \frac{1}{2} \times \frac{i_c \times t_c}{t_c + t_a} = \frac{1}{2} \times \frac{i_c}{r+1} \tag{34}$$

So,

$$i_c = 4i_{av} \quad \text{if } t_a = t_c \tag{35}$$

During the cathodic time of mandrel, $0 < t \leqslant t_c$,

$$i(u) = \frac{i_c}{zFD} \times \left(\frac{-2u}{\theta} + 1\right) \tag{36}$$

By substituting Equation 36 into Equation 20, the change in concentration is

$$\frac{c_e}{c_0} = 1 + \frac{4i_c}{zFc_0\delta}\sum_{n=1}^{\infty}\frac{1}{p^4a^2\theta}[1 - p^2at - \exp(-p^2at)] \tag{37}$$

During the pause time, $t_c < t \leq t_a$, the change in concentration is again found to be the same as in Equation 27.

(d) *For a triangular waveform with relaxation time, W_{tri}*

$$i(t) = \begin{cases} \frac{4i_c t}{\theta} - 4mi_c \\ \qquad \text{for } m\theta < t \leqslant \left(2m + \frac{1}{r+1}\right)\frac{\theta}{2} \\ \frac{-4i_c t}{\theta} + 2i_c + 4mi_c \\ \qquad \text{for } \left(2m + \frac{1}{r+1}\right)\frac{\theta}{2} < t \leqslant \left(m + \frac{1}{r+1}\right)\theta \\ 0 \quad \text{for } \left(m + \frac{1}{r+1}\right)\theta < t \leqslant (m+1)\theta \end{cases} \tag{38}$$

$$i_{av} = \frac{1}{2} \times \frac{i_c \times t_c}{t_c + t_a} = \frac{1}{2} \times \frac{i_c}{r+1} \tag{39}$$

So,

$$i_c = 4i_{av} \quad \text{if } t_a = t_c \tag{40}$$

During the first cathodic time of mandrel, $0 < t \leqslant \frac{t_c}{2}$,

$$i(u) = \frac{i_c}{zFD} \times \frac{4u}{\theta} \tag{41}$$

By substituting Equation 41 into Equation 20, the change in concentration becomes:

$$\frac{c_e}{c_0} = 1 + \frac{8i_c}{zFc_0\delta} \sum_{n=1}^{\infty} \frac{1}{p^4 a^2 \theta} [p^2 at - 1 + \exp(-p^2 at)] \tag{42}$$

During the second cathodic time of mandrel, $\frac{t_c}{2} < t \leqslant t_c$,

$$i(u) = \frac{i_c}{zFD} \times \left(\frac{-4u}{\theta} + 2\right) \tag{43}$$

By substituting Equation 43 into Equation 20, the change in concentration is

$$\frac{c_e}{c_0} = 1 + \frac{16i_c}{zFc_0\delta} \sum_{n=1}^{\infty} \frac{1}{p^4 a^2 \theta} [1 - p^2 at - \exp(-p^2 at)] \tag{44}$$

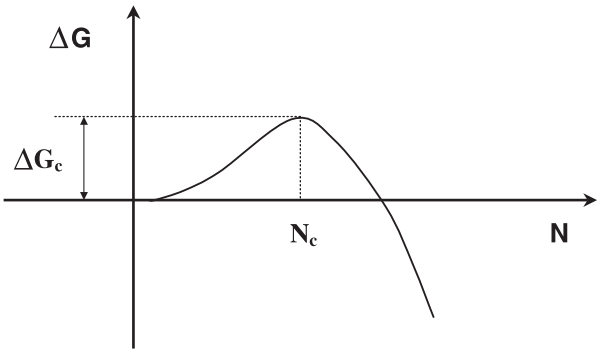

Fig. 1. Free energy of formation of a cluster as a function of size N (a cluster of N atoms); N_c is the size of the critical cluster (nucleus).

During the pause time, $t_c < t \leqslant t_a$, the change in concentration is again the same as in Equation 27.

2.3. *Nucleation and surface nuclei*

The nucleation law for a uniform probability with time t of conversion of a site on the metal electrode into nuclei is given by

$$N = N_0[1 - \exp(-At)] \tag{45}$$

where N_0 is the total number of sites (the maximum possible number of nuclei on the unit surface) and A is the nucleation rate constant. This equation represents the first-order kinetics model of nucleation. The rate of 2D nucleation, J, is given by [31]:

$$J = k_1 \exp\left[-\frac{bs\varepsilon^2}{zekT|\eta|}\right] \tag{46}$$

2.4. *Concentration overpotential*

With diffusion control [32], the concentration differences across the diffusion layer give rise to a concentration overpotential, η_c, which is given by [33–35]:

$$\eta_c = \frac{RT}{zF} \ln\left(\frac{c_e}{c_0}\right) \tag{47}$$

Alternatively, Equation 47 can be written as

$$\eta_c = \frac{RT}{zF} \ln\left(1 - \frac{i}{i_L}\right) \tag{48}$$

The concentration overpotential $\eta_{c,rec}$ can be found by substituting Equations 25 and 27 into Equation 47. The concentration overpotential $\eta_{c,rup}$ can be obtained by substituting Equations 32 and 27 into Equation 47. Likewise, by substituting Equations 37 and 27 into Equation 47, the concentration overpotential $\eta_{c,rdn}$ can be found. Similarly, the concentration overpotential $\eta_{c,tri}$ can be found by substituting Equations 42, 44 and 27 into Equation 47. Since η_0 and η_s can be neglected, the nucleation rates J_{rec}, J_{rup}, J_{rdn}, and J_{tri} can be found by substituting $\eta_{c,rec}$, $\eta_{c,rup}$, $\eta_{c,rdn}$, and $\eta_{c,tri}$ into Equation 46. All these results are shown in Table 1. As shown in the simulation of dimensionless surface concentration of nickel ions during pulse-on-time in Figure 2, the shortest transition time was obtained when W_{rdn} was employed [36]. The longest transition time was obtained when W_{rec} was used. The order of transition time, τ, obtained for different types of waveform is as follows: $\tau_{rdn} < \tau_{tri} < \tau_{rup} < \tau_{rec}$.

When the transition time is reached during pulse plating, the concentration overpotential increases significantly and this results in a total increase in overpotential [29–31]. An increase in the total overpotential

Table 1. Tabulation of nucleation rate, J, for W_{rec}, W_{rup}, W_{rdn}, W_{tri}

Waveform	Time interval	Concentration overpotential, η_c	Nucleation rate, J
W_{rec}	$0 < t \leqslant t_c$	$\frac{RT}{zF}\ln\left(1+\frac{8}{\pi^2}\frac{i_c\delta}{zFD}\sum_{n=1}^{\infty}\frac{1-\exp(-p^2at)}{p^2}\right)$	$k_1\exp\left[-bs\varepsilon^2\Big/zekT\left\lvert\frac{RT}{zF}\ln\left(1+\frac{8}{\pi^2}\frac{i_c\delta}{zFD}\sum_{n=1}^{\infty}\frac{1-\exp(-p^2at)}{p^2}\right)\right\rvert\right]$
	$t_c < t \leqslant t_a$	$\frac{RT}{zF}\ln\left(1+\frac{2i_c}{zF\delta}\sum_{n=1}^{\infty}\frac{\exp[-p^2a(t-t_c)]-\exp(-p^2at)}{p^2a}\right)$	$k_1\exp\left[-bs\varepsilon^2\Big/zekT\left\lvert\frac{RT}{zF}\ln\left(1+\frac{2i_c}{zF\delta}\sum_{n=1}^{\infty}\frac{\exp[-p^2a(t-t_c)]}{p^2a}\right)\right\rvert\right]$
W_{rup}	$0 < t \leqslant t_c$	$\frac{RT}{zF}\ln\left(1+\frac{4i_c}{zF\delta}\sum_{n=1}^{\infty}\frac{1}{p^2a^2\theta}[p^2at-1+\exp(-p^2at)]\right)$	$k_1\exp\left[-bs\varepsilon^2\Big/zekT\left\lvert\frac{RT}{zF}\ln\left(1+\frac{4i_c}{zF\delta}\sum_{n=1}^{\infty}\frac{1}{p^4a^2\theta}[p^2at-1+\exp(-p^2at)]\right)\right\rvert\right]$
	$t_c < t \leqslant t_a$	$\frac{RT}{zF}\ln\left(1+\frac{2i_c}{zF\delta}\sum_{n=1}^{\infty}\frac{\exp[-p^2a(t-t_c)]-\exp(-p^2at)}{p^2a}\right)$	$k_1\exp\left[-bs\varepsilon^2\Big/zekT\left\lvert\frac{RT}{zF}\ln\left(1+\frac{2i_c}{zF\delta}\sum_{n=1}^{\infty}\frac{\exp(-p^2a(t-t_c)}{p^2a}\right)\right\rvert\right]$
W_{rdn}	$0 < t \leqslant t_c$	$\frac{RT}{zF}\ln\left(1+\frac{4i_c}{zF\delta}\sum_{n=1}^{\infty}\frac{1}{p^4a^2\theta}[1-p^2at-\exp(-p^2at)]\right)$	$k_1\exp\left[-bs\varepsilon^2\Big/zekT\left\lvert\frac{RT}{zF}\ln\left(1+\frac{4i_c}{zF\delta}\sum_{n=1}^{\infty}\frac{1}{p^4a^2\theta}[1-p^2at-\exp(-p^2at)]\right)\right\rvert\right]$
	$t_c < t \leqslant t_a$	$\frac{RT}{zF}\ln\left(1+\frac{2i_c}{zF\delta}\sum_{n=1}^{\infty}\frac{\exp[-p^2a(t-t_c)]-\exp(-p^2at)}{p^2a}\right)$	$k_1\exp\left[-bs\varepsilon^2\Big/zekT\left\lvert\frac{RT}{zF}\ln\left(1+\frac{2i_c}{zF\delta}\sum_{n=1}^{\infty}\frac{\exp[-p^2a(t-t_c)}{p^2a}\right)\right\rvert\right]$
W_{tri}	$0 < t \leqslant \frac{t_c}{2}$	$\frac{RT}{zF}\ln\left(1+\frac{8i_c}{zF\delta}\sum_{n=1}^{\infty}\frac{1}{p^4a^2\theta}[p^2at-1+\exp(-p^2at)]\right)$	$k_1\exp\left[-bs\varepsilon^2\Big/zekT\left\lvert\frac{RT}{zF}\ln\left(1+\frac{8i_c}{zF\delta}\sum_{n=1}^{\infty}\frac{1}{p^4a^2\theta}[p^2at-1+\exp(-p^2at)]\right)\right\rvert\right]$
	$\frac{t_c}{2} < t \leqslant t_c$	$\frac{RT}{zF}\ln\left(1+\frac{16i_c}{zF\delta}\sum_{n=1}^{\infty}\frac{1}{p^4a^2\theta}[1-p^2at-\exp(-p^2at)]\right)$	$k_1\exp\left[-bs\varepsilon^2\Big/zekT\left\lvert\frac{RT}{zF}\ln\left(1+\frac{16i_c}{zF\delta}\sum_{n=1}^{\infty}\frac{1}{p^4a^2\theta}[1-p^2at-\exp(-p^2at)]\right)\right\rvert\right]$
	$t_c < t \leqslant t_a$	$\frac{RT}{zF}\ln\left(1+\frac{2i_c}{zF\delta}\sum_{n=1}^{\infty}\frac{\exp[-p^2a(t-t_c)]-\exp(-p^2at)}{p^2a}\right)$	$k_1\exp\left[-bs\varepsilon^2\Big/zekT\left\lvert\frac{RT}{zF}\ln\left(1+\frac{2i_c}{zF\delta}\sum_{n=1}^{\infty}\frac{\exp[-p^2a(t-t_c)]}{p^2a}\right)\right\rvert\right]$

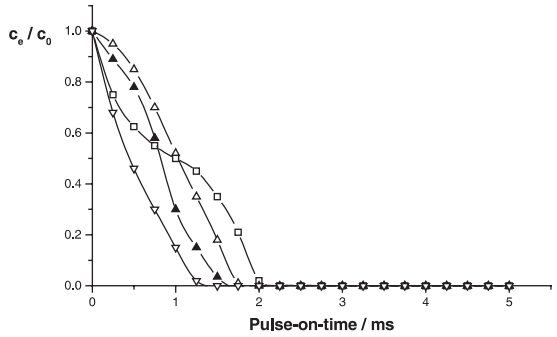

Fig. 2. Simulation of dimensionless surface concentration of nickel ions during pulse-on-time. (Assume $D = 4.7 \times 10^{-6}\,\mathrm{cm\,s^{-1}}$, $\delta = 100\,\mu\mathrm{m}$, $i_{av} = 500\,\mathrm{mA\,cm^{-2}}$ and $t_c = t_a = 5$ ms). (-△-) Ramp-up waveform with relaxation time, (-□-) Rectangular waveform with relaxation time, (-▲-) Triangular waveform with relaxation time, and (-▽-) Ramp-down waveform with relaxation time.

enhances the rate of nucleation. As a result, a deposit with small grain sizes is produced. Thus, the pulse current shape with shorter transition time will produce deposits with finer grain sizes. The finest grain size is produced by utilizing W_{rdn}, since it has the shortest transition time.

To simplify the analysis, it is assumed that the cathodic time of the mandrel, t_c, is equal to the pause time, t_a, and the average current density, i_{av}, is fixed.

By substituting Equations 23, 31, 35 and 40 into Equation 48, respectively, the relationship of concentration overpotential among different types of waveform can be written as

$$\eta_{rec} = \frac{RT}{zF}\ln\left[1 - 2\left(\frac{i_{av}}{i_L}\right)\right] \tag{49}$$

$$\eta_{rup} = \frac{RT}{zF}\ln\left[1 - 4\left(\frac{i_{av}}{i_L}\right)\right] \tag{50}$$

$$\eta_{rdn} = \frac{RT}{zF}\ln\left[1 - 4\left(\frac{i_{av}}{i_L}\right)\right] \tag{51}$$

$$\eta_{tri} = \frac{RT}{zF}\ln\left[1 - 4\left(\frac{i_{av}}{i_L}\right)\right] \tag{52}$$

So,

$$\eta_{rec} < \eta_{rup} \quad \text{while} \quad \eta_{rup} = \eta_{rdn} = \eta_{tri}$$

In an electrocrystallization process, nucleation is enhanced by increasing overpotential. With reference to Puippe [9], the nucleation rate, J, can be simplified as

$$J = k_1 \exp\left(\frac{-k_2}{|\eta|}\right) \tag{53}$$

The ohmic overpotential and the surface overpotential can be neglected. Hence, by substituting Equations 49, 50, 51 and 52 into Equation 53, respectively, the relationship of nucleation rate among different types of waveform can be written as

$$J_{rec} = k_1 \exp\left[\frac{-zFk_2}{\left|RT\ln\left(1 - \frac{2i_{av}}{i_L}\right)\right|}\right] \tag{54}$$

$$J_{rup} = k_1 \exp\left[\frac{-zFk_2}{\left|RT\ln\left(1 - \frac{4i_{av}}{i_L}\right)\right|}\right] \tag{55}$$

$$J_{rdn} = k_1 \exp\left[\frac{-zFk_2}{\left|RT\ln\left(1 - \frac{4i_{av}}{i_L}\right)\right|}\right] \tag{56}$$

$$J_{tri} = k_1 \exp\left[\frac{-zFk_2}{\left|RT\ln\left(1 - \frac{4i_{av}}{i_L}\right)\right|}\right] \tag{57}$$

So,

$$J_{rec} < J_{rup} \quad \text{while} \quad J_{rup} = J_{tri} = J_{rdn}$$

Comparing Equations 54–57, the finer grain sizes can be obtained by utilizing a ramp-up waveform, a ramp-down waveform or a triangular waveform, both with relaxation time. This is because, as shown in Equations 23, 30, 35 and 40, at the same average current density, a higher cathodic peak current density is obtained by utilizing a ramp-up waveform with relaxation time, a ramp-down waveform with relaxation time or a triangular waveform with relaxation time. In these cases the amplitude of the cathodic peak current density is higher and the overpotential becomes larger, which favours the formation of new crystal nuclei rather than the building

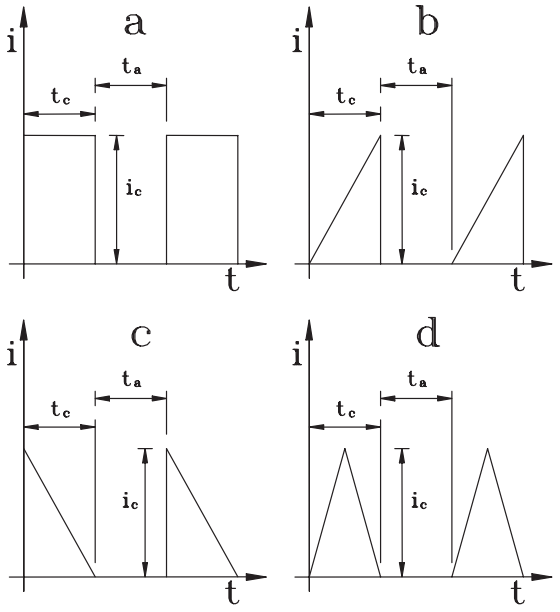

Fig. 3. Different types of waveform: (a) a rectangular waveform with relaxation time, (b) a ramp-up waveform with relaxation time, (c) a ramp-down waveform with relaxation time, and (d) a triangular waveform with relaxation time.

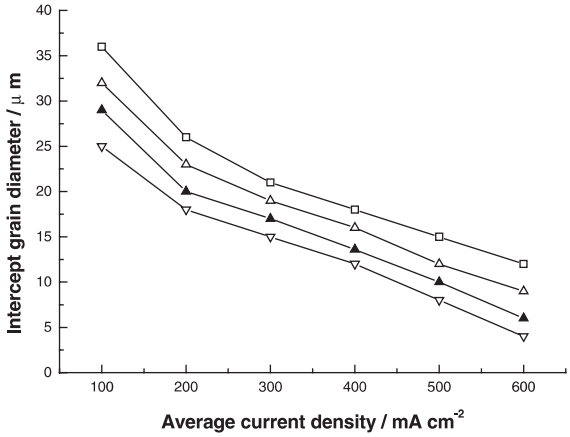

Fig. 4. Effect of different types of waveform on grain size. (-△-) Ramp-up waveform with relaxation time, (-□-) Rectangular waveform with relaxation time, (-▲-) Triangular waveform with relaxation time, and (-▽-) Ramp-down waveform with relaxation time.

up of existing crystals, and hence a decrease in the grain size of the deposit can be expected.

3. Experimental procedures

In the electroforming experiments, the composition of the bath solution was nickel sulphamate 330 g dm^{-3}, nickel chloride 15 g dm^{-3}, boric acid 30 g dm^{-3} and sodium dodecyl sulphate 0.2 g dm^{-3}. The electrolyte was gently agitated by means of a magnetic stirrer, and the temperature was kept at 50 ± 1 °C. The initial pH of the electrolyte was 4.2, a typical value used in electroforming. The cathode mandrel was made of stainless steel with dimensions of 100 mm × 30 mm × 1 mm, and was ground to a finish on grade 180 emery papers. After electroforming, the surface morphology of the electroform of each specimen was examined by SEM. The grain sizes were measured in accordance with ASTM E112-95. Each specimen was subjected to microhardness testing according to ASTM E384.

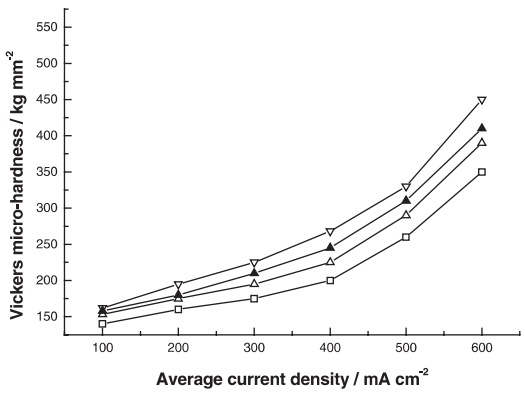

Fig. 5. Effect of different types of waveform on hardness value. (-△-) Ramp-up waveform with relaxation time, (-□-) Rectangular waveform with relaxation time, (-▲-) Triangular waveform with relaxation time, and (-▽-) Ramp-down waveform with relaxation time.

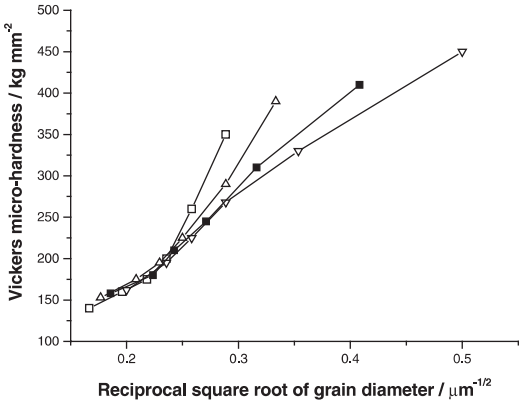

Fig. 6. Relationship between hardness and grain size. (-△-) Ramp-up waveform with relaxation time, (-□-) Rectangular waveform with relaxation time, (-▲-) Triangular waveform with relaxation time, and (-▽-) Ramp-down waveform with relaxation time.

The different types of complex waveform of pulse current generated by a pulse generator are shown in Figure 3. They are defined by the cathodic time of the mandrel (t_c), the off-time (t_a), the cathodic peak current density (i_c), and the period of one cycle (θ).

The pulse frequency was kept constant at 100 Hz, and the electrodeposition thickness was fixed at 200 μm.

4. Results and discussions

Figure 4 shows that, at the same average current density, a much coarser grain size was obtained when a

Table 2. Effect of applying different types of waveform on the microhardness at the same average current density

Average current density /mA cm^{-2}	Type of waveform	Vickers microhardness /kg mm^{-2}	Grain diameter /μm	Reciprocal square root of grain diameter /$\mu m^{-1/2}$
100	W_{rec}	140	36	0.166 667
	W_{rup}	153	32	0.176 777
	W_{rdn}	162	25	0.200 000
	W_{tri}	158	29	0.185 695
200	W_{rec}	160	26	0.196 116
	W_{rup}	175	23	0.208 514
	W_{rdn}	195	18	0.235 702
	W_{tri}	180	20	0.223 607
300	W_{rec}	175	21	0.218 218
	W_{rup}	195	19	0.229 416
	W_{rdn}	225	15	0.258 199
	W_{tri}	210	17	0.242 536
400	W_{rec}	200	18	0.235 702
	W_{rup}	225	16	0.250 000
	W_{rdn}	268	12	0.288 675
	W_{tri}	245	13.6	0.271 163
500	W_{rec}	260	15	0.258 199
	W_{rup}	290	12	0.288 675
	W_{rdn}	330	8	0.353 553
	W_{tri}	310	10	0.316 228
600	W_{rec}	350	12	0.288 675
	W_{rup}	390	9	0.333 333
	W_{rdn}	450	4	0.500 000
	W_{tri}	410	6	0.408 248

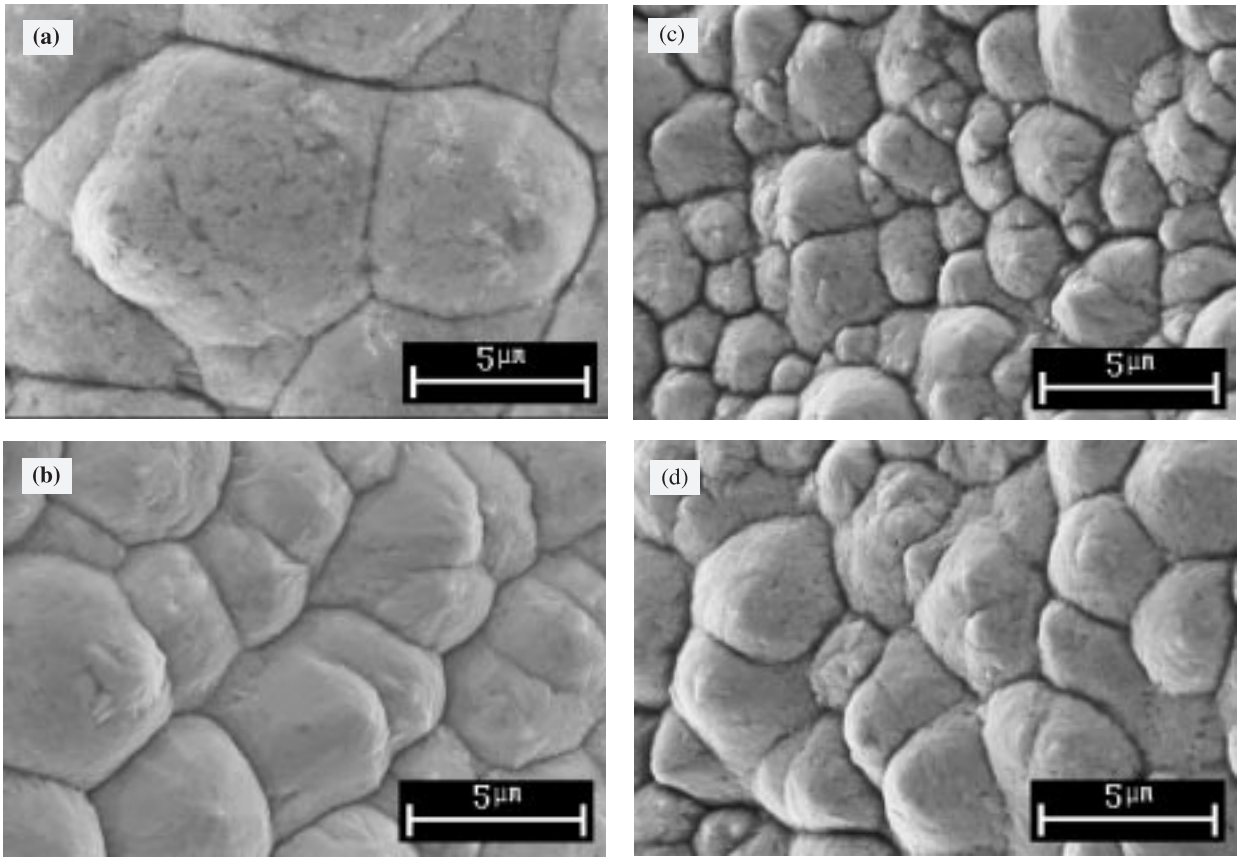

Fig. 7. SEM photos showing the surface morphology of the deposits obtained at a fixed electrodeposition thickness with an average current density of 500 mA cm^{-2}: (a) a rectangular waveform with relaxation time, (b) a ramp-up waveform with relaxation time, (c) a ramp-down waveform with relaxation time, and (d) a triangular waveform with relaxation time.

conventional rectangular waveform with relaxation time, W_{rec}, was employed, while some improvement was achieved when either a ramp-up waveform with relaxation time, W_{rup}, or a triangular waveform with relaxation time, W_{tri}, was used. The finest grain size was obtained by using a ramp-down waveform with relaxation time, W_{rdn}. The order of grain size, d, obtained for different types of waveform is as follows: $d_{rdn} < d_{tri} < d_{rup} < d_{rec}$.

Figure 5 shows that at the same average current density, a much lower hardness value was obtained when a W_{rec} was employed, while some improvement was achieved when either a W_{rup} or a W_{tri} was used. The highest hardness was obtained by utilizing a W_{rdn}. The hardness value, H, measured for the different types of waveform is in the following order: $H_{rdn} > H_{tri} > H_{rup} > H_{rec}$.

Figure 6 shows that at the same average current density, Hall–Petch behaviour was found for the cases of W_{rdn} and W_{tri}. The effect of applying different types of waveform on the microhardness is shown in Table 2.

Therefore, in order to obtain the finest grain size and the highest hardness, i_{rdn} should be applied in the pulse current electroforming of nickel. This is because the highest cathodic peak current density i_{rdn} generates the highest overpotential, which favours the formation of new crystal nuclei rather than the building up of existing crystals, and hence produces the finest grain sizes. Some typical examples showing the surface morphology of the electroforms are shown in Figures 7(a), (b), (c) and (d). These are in agreement with the theoretical predictions.

5. Conclusions

The effects of different types of waveform on the hardness and grain size of nickel electroforms have been studied experimentally and theoretically. According to the experimental findings, at a fixed average current density, a constant pulse period, and a fixed electrodeposition thickness, the highest hardness was obtained when a ramp-down waveform with relaxation time was used. Analytical equations for overpotential and nucleation rate related to the hardness improvement at a fixed electrodeposition thickness and a constant average current density were derived, and the experimental findings are consistent with the theoretical predictions.

Acknowledgement

Financial support for the project, under the code V668, from the Hong Kong Polytechnic University is gratefully acknowledged.

References

1. A.M. Ozerov, N.P. Litvishko, I.N. Vavilina, P.M. Chetvertnov and Ya.E. Zhak, *J. Appl. Chem.* **40** (1967) 1101.
2. H.Y. Cheh, *J. Electrochem. Soc.*: *Electorchem. Sci.* **118** (1971) 551.
3. K. Viswanathan and H.Y. Cheh, *J. Electrochem. Soc.*: *Electorchem. Sci.* **125** (1978) 1616.
4. N. Ibl, *Surf. Technol.* **10** (1980) 81.
5. K.P. Wong, MSc Dissertation, The Hong Kong Polytechnic University (1998).
6. A.R. Despic and K.I. Popov, *J. Appl. Electrochem.* **1** (1971) 275.
7. V.V. Romanow, *Zh. Prikl. Khim.* **36**(5) (1963) 1050–1063.
8. A.J. Avila and M.J. Brown, *Plating* (*East Orange*, *NJ*) **57**(11) (1970) 1105.
9. J.C. Puippe and F. Leaman, 'Theory and Practice of Pulse Plating', American Electroplaters and Surface Finishers Society (1986).
10. N. Ibl, Proceedings of the International Conference on 'Protection against Corrosion by Metal Finishing' (1967) 48.
11. N. Ibl, J.Cl. Puippe and H. Angerer, *Surf. Technol.* **6** (1978) 287.
12. G.A. DiBari, *Plat. Surf. Finish.* **84**(8) (1997) 60.
13. K.P. Wong, K.C. Chan and T.M. Yue, *Surf. Coat. Technol.* **115**(2, 3) (1999) 132.
14. M.A. Otooni, R.W. Armstrong, N.J. Grant and K. Ishizaki, Material Research Society Symposium Proceedings (Vol. 362): 'Grain Size and Mechanical Properties – Fundamentals and Applications' (1995).
15. J.H. Westbrook and H. Conrad, The Science of Hardness Testing and Its Research Applications (American Society for Metals, OH, 1973).
16. M.F. Ashby and David R.H. Jones, 'Engineering Materials: An Introduction to their Properties and Applications' (Pergamon Press, Oxford, 1982).
17. W.D. Callister, 'Material Science and Engineering: An Introduction' (J. Wiley & Sons, 3rd edition, New York, 1994).
18. K. Balakrishnan, J. Kumar and P. Ramasamy, *J. Mater. Sci. Lett.* **14** (1995) 720.
19. V.A. Lamb, *Plating* **56**(8) (1969) 909.
20. V.B. Singh and R.S. Sarabi, *Plat. Surf. Finish.* **83**(10) (1996) 54.
21. E.S. Chen and F.K. Sautter, *Plat. Surf. Finish.* **63**(9) (1976) 28.
22. R.W. Armstrong, Mat. Res. Soc. Symp. Proc. Vol. 362 (Material Research Society, 1995), p. 9.
23. N.J. Petch, *J. Iron Steel Inst.* **174** (1953) 25.
24. M. Paunovic and M. Schlesinger, 'Fundamentals of Electrochemical Deposition' (Electrochemical Society, Pennington, NJ, 1998), Chapter 16.
25. H. McArthur, 'Corrosion Prediction and Prevention in Motor Vehicles' (Ellis Horwood, Chichester, UK, 1988).
26. K. Viswanathan, M.A. Farrell Epstein and H.Y. Cheh, *J. Electrochem. Soc.*: *Electrochem. Sci. & Technol.* **125** (1978) 1772.
27. H.Y. Cheh, *J. Electrochem. Soc.*: *Electrochem. Sci. & Technol.* **118** (1971) 551.
28. J. Crank, 'The Mathematics of Diffusion' (Oxford University Press, New York, 1975), Chapter 4.
29. K.I. Popov, M.D. Maksimivic and M.S. Simic, *Surf. Technol.* **16** (1982) 209.
30. A.R. Despic and K.I. Popov, *Mod. Aspects Electrochem.* **7** (1972) 199.
31. J.O'M Bockris and S.U.M. Khan, 'Surface Electrochemistry – A Molecular Level Approach' (Plenum Press, New York, 1993).
32. E. Raub and K. Muller, 'Fundamentals of Metal Deposition' (Elsevier, New York, 1967).
33. A.M. Bond, 'Modern Polarographic Methods in Analytical Chemistry' (Marcel Dekker, New York, 1980).
34. L. Meiters, 'Polarographic Techniques' (J. Wiley & Sons, New York, 1965).
35. F. Vydra, K. Stulik and E. Julakova, 'Electrochemical Stripping Analysis' (Halsted Press, New York, 1976).
36. D.C. Hanselman, 'Mastering MATLAB 5 – A Comprehensive Tutorial and Reference' (Prentice Hall, NJ, 1998).